geosciences

MDPI

Article

Fluid-Related Features in the Offshore Sector of the Sciacca Geothermal Field (SW Sicily): The Role of the Lithospheric Sciacca Fault System

Dario Civile *, Luca Baradello, Flavio Accaino, Massimo Zecchin, Emanuele Lodolo, Giulia Matilde Ferrante, Nora Markezic, Valentina Volpi and Mihai Burca

National Institute of Oceanography and Applied Geophysics-OGS, 34010 Sgonico, TS, Italy; lbaradello@ogs.it (L.B.); faccaino@ogs.it (F.A.); mzecchin@ogs.it (M.Z.); elodolo@ogs.it (E.L.); gferrante@ogs.it (G.M.F.); nmarkezic@ogs.it (N.M.); vvolpi@ogs.it (V.V.); mburca@ogs.it (M.B.)
* Correspondence: dcivile@ogs.it

Abstract: The Sciacca basin extends in the southwestern part of Sicily and hosts an important geothermal field (the Sciacca Geothermal Field) characterized by hot springs containing mantle gasses. Newly acquired high-resolution seismic profiles (Boomer data) integrated with a multichannel seismic reflection profile in close proximity to the Sciacca Geothermal Field have documented the presence of numerous active and shallow fluid-related features (pipes, bright spots, buried and outcropping mud volcanoes, zones of acoustic blanking, and seafloor fluid seeps) in the nearshore sector between Capo San Marco and Sciacca (NW Sicilian Channel) and revealed its deep tectonic structure. The Sciacca Geothermal Field and the diffuse submarine fluid-related features probably form a single onshore–offshore field covering an area of at least 70 km^2. This field has developed in a tectonically active zone dominated by a left-lateral transpressive regime associated with the lithospheric, NNE-striking Sciacca Fault System. This structure probably favored the rising of magma and fluids from the mantle in the offshore area, leading to the formation of a geothermal resource hosted in the Triassic carbonate succession that outcrops onshore at Monte San Calogero. This field has been active since the lower Pleistocene, when fluid emissions were likely greater than today and were associated with greater tectonic activity along the Sciacca Fault System.

Keywords: shallow marine fluid-related features; seafloor gas seeps; mud volcanoes; lithospheric transpressive fault system; multichannel and high-resolution seismic data; Sciacca Geothermal Field; Sicilian Channel

Citation: Civile, D.; Baradello, L.; Accaino, F.; Zecchin, M.; Lodolo, E.; Ferrante, G.M.; Markezic, N.; Volpi, V.; Burca, M. Fluid-Related Features in the Offshore Sector of the Sciacca Geothermal Field (SW Sicily): The Role of the Lithospheric Sciacca Fault System. *Geosciences* **2023**, *13*, 231. https://doi.org/10.3390/geosciences13080231

Academic Editors: Jesus Martinez-Frias and Andrea Brogi

Received: 26 June 2023
Revised: 26 July 2023
Accepted: 27 July 2023
Published: 31 July 2023

1. Introduction

The Sciacca basin, located in the southern part of western Sicily (Figure 1a), hosts an important geothermal field (the Sciacca Geothermal Field) known since Roman times. This field is fed by a thermal and saline aquifer occurring in the Triassic carbonate succession of Monte San Calogero (known also as Monte Kronio) [1] (Figure 1b). This succession is characterized by a considerable secondary permeability associated with karstification phenomena and tectonic fractures [1,2].

The Sciacca area presents a peculiar tectonic setting, being located at the corner of the outermost thrust front of the Sicilian–Maghrebian chain associated with the active Gela Nappe (e.g., [3]) and the northernmost part of the NNE-oriented Sciacca Fault System (SFS). The SFS forms, together with the Capo Granitola Fault System (CGFS), the main active lithospheric shear zone of the western Sicilian Channel known as the Capo Granitola–Sciacca Fault Zone (e.g., [4–8]) (Figure 1a,b).

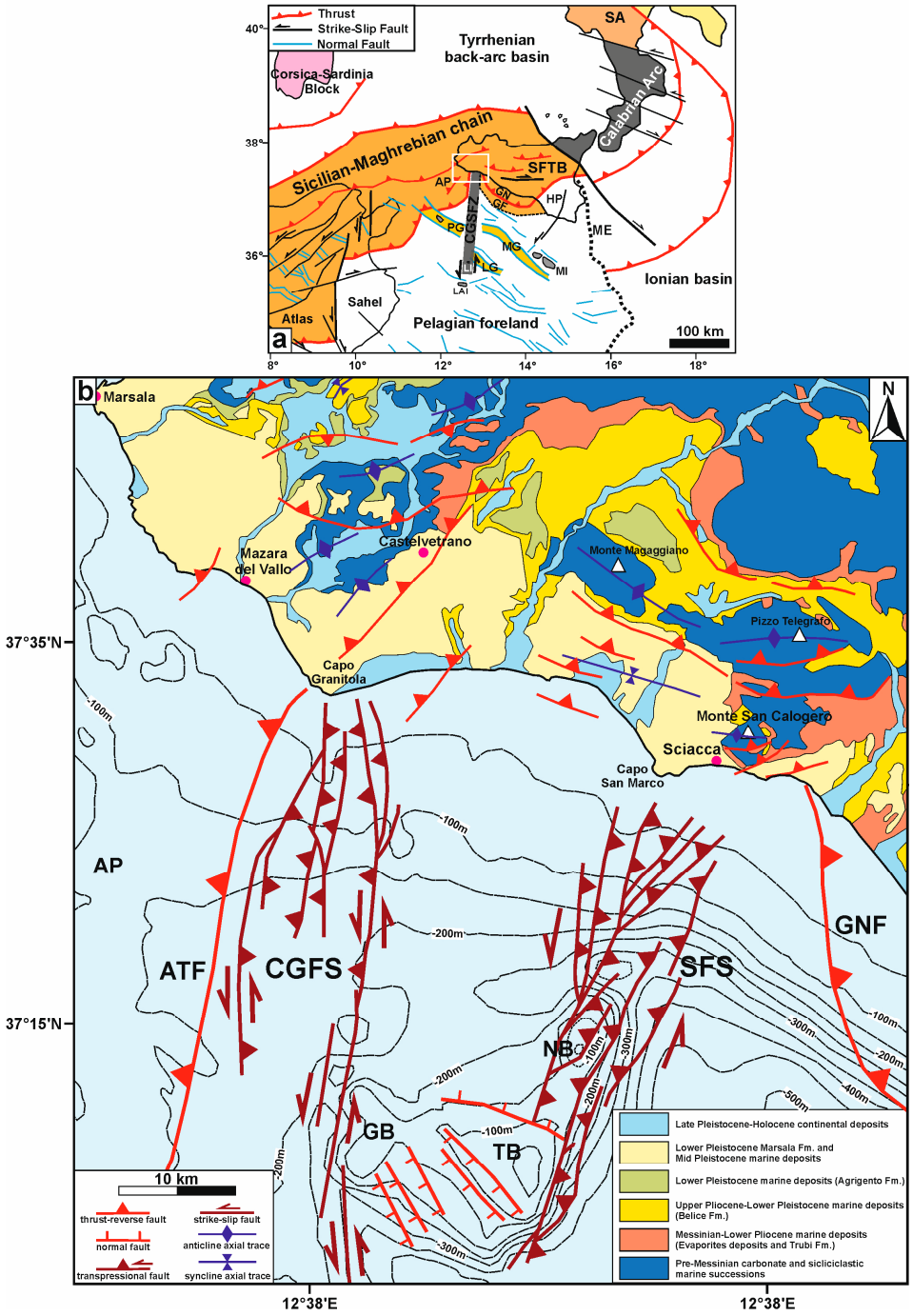

Figure 1. (**a**) Simplified sketch map showing the main geodynamic features of the central Mediterranean area between the Southern Apennines to the north and the Sicilian–Maghrebian chain to the southwest (modified from Civile et al. [7]). The white rectangle is the area reported in (**b**). Abbreviations: AV: Adventure Plateau; CGSFZ: Capo Granitola–Sciacca Fault Zone; GF: Gela Foredeep; GN: Gela Nappe; HP: Hyblean Plateau; LG: Linosa Graben; LAI: Lampedusa Island; LI: Linosa Island; ME: Malta Escarpment; MI: Maltese Islands; PG: Pantelleria Graben: SA: Southern Apennines; SFTB: Sicilian Fold and Thrust Belt. (**b**) Simplified structural map of southwestern Sicily offshore (modified from Civile et al. and Ferranti et al. [6–8]) and onshore (modified from [8]). Bathymetric data derived from the EMODnet Bathymetry Portal from "http://emodnet-bathymetry.eu/" (accessed on 1 June 2023) Digital Terrain Model (1/16*1/16 arcmin grid resolution). Abbreviations: AP: Adventure Plateau; ATF: Adventure Thrust Front; CGFS: Capo Granitola Fault System; GB: Graham Bank; GNF: Gela Nappe Front; NB: Nerita Bank; SFS: Sciacca Fault System; TB: Terrible Bank.

The origin of the thermal waters in the Sciacca basin is still not fully understood, although several interpretative models have been proposed. These generally assume the presence of a generic deep subvertical fault system from which geothermal fluids rise from a mantle magma possibly located offshore (e.g., [9]). Geochemical studies conducted on thermal fluid seeps suggest a significant contribution from mantle-derived gasses [2,9–11].

While most studies on the Sciacca Geotherm Field have been conducted onshore, little is known about the possible presence of fluid upwellings in the immediate offshore area. For this reason, a high-resolution seismic and magnetic survey campaign was recently conducted to identify the possible presence of fluid-related features in the offshore area between the town of Sciacca and Capo San Marco. This campaign complements a high-resolution geophysical survey conducted some years ago immediately west of the study area, where a series of mud volcanoes and pockmarks were recognized and mapped [12,13].

This paper presents the results of the interpretation of these recently collected high-resolution seismic reflection profiles near the Sicilian coast of Sciacca. These data were integrated with a multichannel seismic reflection profile provided by the Italian ViDEPI project (Visibility of Petroleum Exploration Data in Italy, "http://www.videpi.com" (accessed on 22 May 2023), of the Italian Ministry of the Economic Development), which allowed the visualization of the tectonic setting of the SFS and stratigraphic information from literature data and well logs. Here, a link between offshore fluid manifestations and the SFS is hypothesized, as active fault zones can facilitate the ascent of geothermal fluids from depth by keeping fractures open and dynamically maintaining effective permeability in the reservoir, both upward and downward (e.g., [14,15]).

The potentially widespread presence of thermal phenomena in the Sciacca basin, both onshore and offshore, associated with lithospheric-scale tectonic structures, such as the SFS, could stimulate the development of research projects focused on reassessing the potential for low-enthalpy energy power generation in hydrothermal systems in the context of the continued increase in global demand for alternative energy sources.

2. Geological Setting

2.1. Onshore Sciacca Area

Western Sicily is part of the Sicilian fold and thrust belt (SFTB), which is the emerged part of the south-verging Sicilian–Maghrebian chain (Figure 1a). This is a thin-skinned Neogene–Quaternary accretionary wedge developed in the central Mediterranean and progressively migrated southward over the Pelagian–African foreland as a result of the collision between the African and European plates (e.g., [16–20]).

In the southwestern part of Sicily, between the towns of Marsala and Sciacca, two distinct tectonic zones can be identified (Figure 1b): (i) a western part characterized by the presence of NNE-trending, east-verging thrusts and associated ramp anticlines developed in the Mesozoic–Cenozoic Trapanese pelagic carbonate platform and covered by Neogene clastic deposits [9,21,22] and (ii) an eastern part with WNW-trending, south-to-southwest-verging thrusts that form the Monte Magaggiaro, Pizzo Telegrafo, and Monte San Calogero ridges. These ridges are thrust ramp anticlines composed of Mesozoic–Cenozoic carbonates of the Saccense platform [21,23]. The structural highs surround a gently sloping coastal plain composed mainly of lower Pleistocene marine sediments of the Marsala Fm. [21] (Figure 1b). This formation consists of bioclastic calcarenites and calcirudites in the western sector [24,25] that pass to silty clays in the southeast and on the continental shelf [8]. Late Pleistocene–Holocene continental deposits are locally found along the coast, while inland small outcrops of marine calcarenites and sands of the lower Pleistocene Agrigento Fm. are found [21] (Figure 1b). Quaternary deposits unconformably cover upper Pliocene–lower Pleistocene sandstones, clays, and calcarenites of the Belice Marnoso-Arenacea Fm., pelagic marls and calcilutites of the lower Pliocene Trubi Fm., upper Messinian evaporites, and middle-upper Miocene terrigenous deposits [21,23] (Figure 1b).

2.2. Sciacca Geothermal Field

The Sciacca Geothermal Field (SGF) is located in southwestern Sicily within the Sciacca basin (10 km^2), which is roughly equivalent to the area of the town of Sciacca [1] (Figure 2). The SGF is characterized by the widespread occurrence of thermal fluid leaks, which are also discharged in karst caves (known as "stufe"). The latter are located on Monte San Calogero (396 m a.s.l.) and consist of emissions of hot air and vapors. Sixteen different thermal springs, with a maximum temperature of 55 °C [11], and a hundred wells have been documented in the SGF by several authors (e.g., [1,26]).

The origin of the thermal waters of the SGF was debated since the end of the 19th century. Gemmellaro [27,28] and Hoffmann [29] proposed a relationship between the thermalism of the area and the magmatic activity in the Sicilian Channel. Alaimo et al. [30], Alaimo and Tonani [26], and Aureli [1] proposed a geochemical model based on the presence of a deep marine-related reservoir in Triassic carbonate rocks diluted by meteoric water at shallower levels. Favara et al. [31] evaluated the direct link between the thermal springs and the main tectonic structures in western Sicily. These authors suggested for the SGF waters a feeding reservoir composed of 50% carbonate water and 50% seawater, which may interact with NaCl-rich evaporitic layers. Based on helium isotopic ratios, Caracausi et al. [10] suggested that this feature is the result of an outgassing by deep N-S extensional fault systems associated with the accumulation of mantle magma intruded into the continental crust of western Sicily.

For Capaccioni et al. [2], Montanari et al. [9], and Donato et al. [11], geochemical and isotopic evidence from springs and wells of the SGF indicate a deep origin of the Sciacca geothermal reservoir, characterized by a significant amount of mantle gasses. It is likely that the hot and deep thermal fluids circulate at depths of several kilometers and migrate to the surface along subvertical tectonic structures affecting the carbonate successions and are subsequently diluted by a crustal component. According to Montanari et al. [9], it is possible to hypothesize that the mantle magma generating the observed isotopic compositions of CO_2 and He is located offshore.

2.3. Offshore Sciacca Area

The seismic lines presented in this paper are in the northernmost part of the Sicilian Channel (SC) near the coast of Sciacca (Figure 2). SC is a wide shallow water area that represents the northern part of the African continental plate. The western part of the SC is crossed by the Capo Granitola–Sciacca Fault Zone—CGSFZ [6]—an NNE-oriented, left-lateral lithospheric shear zone that extends at least from Linosa Island to the Capo Granitola–Sciacca coast of Sicily [4–8,32–36] (Figure 1a). The northern part of the CGSFZ consists of two fault systems: the CGFS to the west and the SFS to the east (Figure 1b). Both are characterized by the presence of positive flower structures [6,8,35], and there is evidence of Quaternary tectonics [6,8]. The northern part of the CGSFZ separates two sectors of the Sicilian–Maghrebian chain, characterized by different deformation ages, distinct structural trends, and tectonic evolution [4,37–40]. The western sector, that is the Adventure Plateau (Figure 1b), is occupied by Tortonian-lower Messinian deposits of the NE-oriented Adventure Foredeep lying on a Mesozoic–Cenozoic carbonate substrate, was affected by a late Miocene compressional phase [32,38–41], which produced ESE-verging thrusts [42,43]. Evidence of active thrusting has been recognized by Barreca et al. [22] from Castelvetrano village to the Capo Granitola offshore. The eastern sector of the chain consists of the Pliocene–Quaternary WNW-oriented Gela Foredeep Basin, partially buried by the arcuate frontal termination of the Oligocene–Pleistocene Gela Nappe [3,4,33,37,44,45] (Figure 1b). It was affected by Pliocene to Pleistocene superposed compressional deformations [33,46–49].

The Capo Granitola–Sciacca offshore is also characterized by the presence of several small Quaternary monogenic volcanic edifices found on the Graham and Terrible banks and in the nearshore area of the Capo Granitola–Sciacca coast of Sicily, where a broad sill intrusion has also been identified near the Messinian unconformity [50–53] (Figure 2a). The most famous volcanic manifestation was the formation of the ephemeral island of Ferdinandea (Figure 2a) that occurred in 1831 on the Graham Bank [54,55]. The origin of the volcanism in this area has been associated with the rising of magmas along the lithospheric faults of the CGSFZ [6].

The sedimentary succession of the offshore area, reconstructed on the basis of the literature information [6,8,33,43,44,49,56], consists of a Triassic—middle Miocene, mainly carbonate succession overlain by shelf siliciclastic deposits of the Tortonian–lower Messinian Terravecchia Fm. Locally, Messinian evaporites and related sediments of the Gessoso-Solfifera Group can be present. The lower part of the Pliocene–Quaternary succession, which lies on the Messinian unconformity, consists of pelagic marls and marly limestones of the Zanclean Trubi Fm., which is covered by Piacenzian–Pleistocene clayey shelf deposits with sandy intercalations of the Ribera Fm.

2.4. Gas Presence and Related Features in the Capo Granitola–Sciacca Offshore

Recent works by Ferrante et al. [12] and Volpi et al. [13] have documented the presence of gas and related features both in the subsurface and at the seafloor in the Capo Granitola–Sciacca offshore area based on high-resolution bathymetric data and seismic profiles. Also, Barreca et al. [22] showed the possible occurrence of cold seeps in the offshore of Capo Granitola based on high-resolution seismic profiles. Ferrante et al. [12] also identified these features by analyzing amplitude and velocity anomalies in the Miocene–Pliocene sedimentary succession.

Buried and outcropping mud volcanoes, with maximum extents and heights of 0.155 km^2 and 10 m, respectively, were identified along the northern part of the CGFZ and SFS (Figure 2a). These mounds exhibit opaque seismic facies with no visible internal reflectors and are sometimes associated with gas emissions in the water column, bright spots, and zones of signal blanking in the subsurface. The mounds located along the SFS form a 2 km long field characterized by an approximate N-S trend [12,13] (Figure 2a). Another gas expression visible on the seafloor and in the high-resolution seismic profiles is represented by pockmarks. A wide pockmark field composed of over 40 depressions, extends for 25 km with an NW-SE direction between the Nerita Bank and the CGFS [12,13] (Figure 2a). Gas-related features, such as bright spots, gas chimneys, and a dimmed amplitude zone, were identified in the whole Miocene–Pleistocene succession [12]. These authors suggest a thermogenic deep origin for the observed gas. It may have been generated by shaly-marly intercalations of the Meso-Cenozoic carbonate succession and then migrated upward through faults associated with the lithospheric CGSFZ.

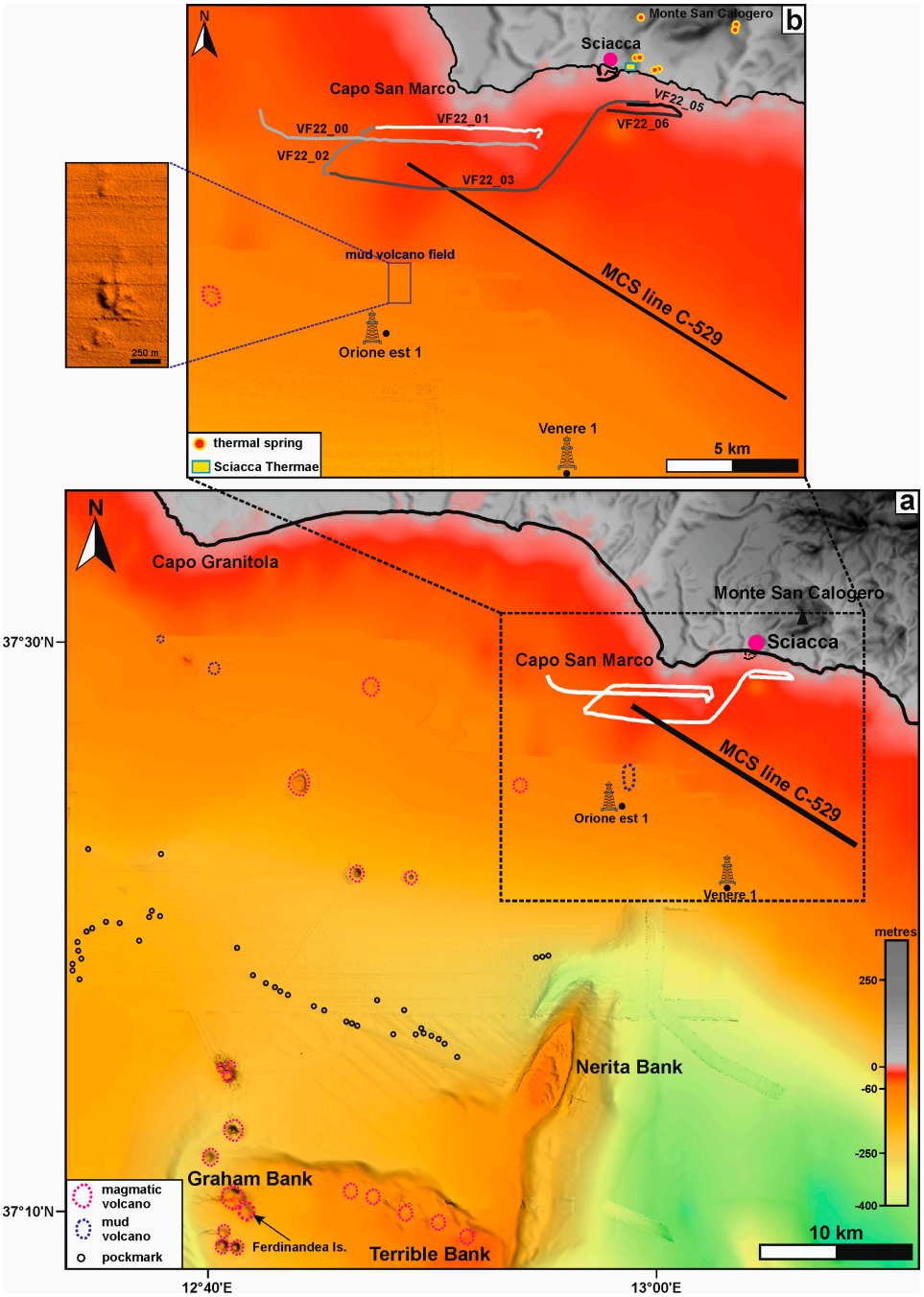

Figure 2. (**a**) Morpho–bathymetric map of the NW part of the Sicilian Channel, covering the offshore area between the Capo Granitola–Sciacca coast of Sicily and the Graham and Terrible banks, and the onshore coastal area. Data from the EMODnet Bathymetry Portal (http://emodnet-bathymetry.eu/) Digital Terrain Model (1/16*1/16 arcmin grid resolution) and multibeam data collected in 2018 by OGS. The location of volcanic edifices, mud volcanoes, and pockmarks (from [6,12,13,50,51]) is indicated along with the location of the October 2022 high–resolution geophysical survey (VF lines), the multichannel seismic line C–529, and the two exploration wells Orione est 1 and Venere 1 available from the ViDEPI project. (**b**) Detail of the Capo San Marco–Sciacca area showing the position of the six high-resolution seismic reflection profiles acquired in October 2022 (white lines) and the multichannel seismic line C–529 (black line). In addition, a detailed bathymetry (box on the left) of the mud volcano field located south of Capo San Marco [12] and the location of the main onshore thermal springs in the area encompassing the town of Sciacca and Monte San Calogero are shown.

3. Materials and Methods

The geophysical dataset used in this work consists of:

- Six high-resolution seismic reflection profiles (Boomer system) (Figure 2b) and magnetic data acquired in October 2022 in the offshore area between Sciacca and Capo San Marco.

- A part of the NW-SE-oriented multichannel seismic reflection profile C529, located a few kilometers (4–7 km) from the Sicilian coast between Capo San Marco and Sciacca (Figure 2), which was used to image the deep structure of the SFS. This line was calibrated using the "Orione est 1" and "Venere 1" wells, which are included in the ViDEPI Project.

The seismo-stratigraphic and structural interpretation of a geophysical dataset was performed using the software Kingdom™ version 2021 from IHS Markit®. The recognition of seismic units is based on their bounding discontinuities, geometries and stratal architecture, and seismic characters (amplitude, lateral continuity, and frequency of internal reflectors).

The Boomer system consists of an electrodynamic transducer mounted on a catamaran frame and a pre-amplified solid streamer consisting of 10 hydrophones connected in series. Each hydrophone can be switched on/off, extending the active part from 1 m to 10 m. During acquisition, the length of the active part was kept lower than the water depth to avoid aliasing in the reflection signals, since it is the sum of the array without normal move out correction. The distance between the source and the streamer (offset) was 20 m. The shooting rate of the plate (the energy unit powered 300 J/pulse) was two shots per second, and the reflected signal was sampled at 0.05 ms with a time window of 400 ms. Data were acquired using SB-Logger, a 24-bit sigma/delta converter, and saved in an SEG-Y format file. Profiles were tracked using a navigator connected to a differential GPS, which ensured accurate positioning of the traces. Data processing, performed with Echos™ version 2015 from Emerson Paradigm®, included gain recovery (a spherical divergence and amplitude recovery obtained by inverting the amplitude decay curve), time-variant bandpass filters, a 2D filter, and predictive deconvolution. In addition, after true amplitude processing, the instantaneous amplitude was calculated using the free Seismic Unix* software [57] version SU 43R1 2012 for parts of the high-resolution seismic lines to analyze reflectivity anomalies of the reflections. Differences in reflectivity can provide information about the nature of the sediments both on the seafloor and in shallower subsurface levels.

Magnetic data were acquired using a SeaSpy® marine magnetometer with a maximum ideal resolution of 0.001 nT and a sampling rate of 1 s. Magnetic anomalies were determined by removing the International Geomagnetic Reference Field (IGRF) and diurnal effects caused by variations in the external magnetic field. The diurnal effects were corrected by using data from the Lampedusa Magnetic Observatory managed by INGV.

The C-529 multichannel seismic reflection profile was downloaded from the ViDEPI project. This line belongs to the Italian Commercial Zone "C" and was collected by ENI in 1968. The seismic line, available as an image file (PDF format), was converted to the SEG-Y file using the open-source Seismic Unix* software, sampling the image on the basis of trace number and time sampling of the original file. Then, the SEG-Y file was edited to assign the CMP (common mid-points) to the corresponding geographic coordinates. To reconstruct the seismic section as faithfully as possible, bandpass filters were applied to the SEG-Y file following the processing of information contained in the original file. Post-stack time migration was applied to the SEG-Y file to remove diffractions and better define the slope of the reflections.

4. Results of the Seismic Data Interpretation

4.1. MCS Line C-529

This seismic line shows the deep tectonic setting of the Sciacca offshore, characterized from NW to SE by the following three structural domains (Figure 3): the Sciacca Fault System (SFS), the Gela Foredeep Basin (GFB), and the Gela Nappe (GN).

4.1.1. Seismic Stratigraphy

Two prominent reflectors were recognized: the Messinian unconformity (MU in Figure 3) and the top of the Mesozoic–Cenozoic carbonate succession (TCS in Figure 3). MU is seismically expressed by a continuous high-amplitude reflector that is well recognized and probably associated with a subaerial exposure (Messinian erosional surface, MES). TCS marks an important lithologic change between siliciclastic and carbonate successions above and below this horizon, respectively, and consists of a high-amplitude, laterally discontinuous reflector affected by considerable tectonic deformation. Another medium-amplitude and laterally continuous reflector (TT in Figure 3) is clearly visible in the seismic line at the top of a semi-transparent seismic unit associated with deposits known in Sicily as Trubi Fm.

Four seismic stratigraphic units (labeled from younger to older as US1 to US4 in Figure 3) were identified.

Weakly tectonized Unit S1 (US1) consists of well-layered, laterally continuous, and parallel reflectors with low- to high-amplitude and medium- to high-frequency. Based on literature information (e.g., [6,8,49]) and available boreholes (Oscar 1 Est and Venere 1; see Figure 3), Unit S1 is correlated with the clayey shelf deposits with silty and sandy intercalations of the upper Pliocene–Pleistocene Ribera Fm. (corresponding to the Marsala Fm. onshore) and its deeper part with the Belice Marnoso-Arenacea Fm. The maximum thickness, considering an interval velocity of 1800 m/s [6], ranges from a few hundred meters to over 1500 m in the sector of the GFB near GN (Figure 3).

Unit S2 (US2) is characterized by semi-transparent seismic facies consisting of discontinuous low-amplitude reflectors. This seismic signature is generally well recognized and is associated with the lower Pliocene pelagic marls and marly limestones of the Trubi Fm. Their thickness varies from a few tens of meters, at the top of the SFS, to over 250 m (Figure 3), considering an interval velocity of 2100 m/s [6].

Unit S3 (US3) consists of low- to medium-frequency, low- to high-amplitude, and generally discontinuous reflectors, but a semi-transparent chaotic seismic facies is also locally visible. This unit is mainly associated with the siliciclastic shelf deposits of the Tortonian–lower Messinian Terravecchia Fm. It is characterized by significant thickness variations from 300 to over 800 m (Figure 3) considering an interval velocity of 2300 m/s [6].

Unit S4 (US4) comprises the Mesozoic–Cenozoic carbonate succession, which is generally affected by significant tectonic deformation. This unit may have chaotic seismic facies or highly discontinuous low- to high-amplitude reflectors.

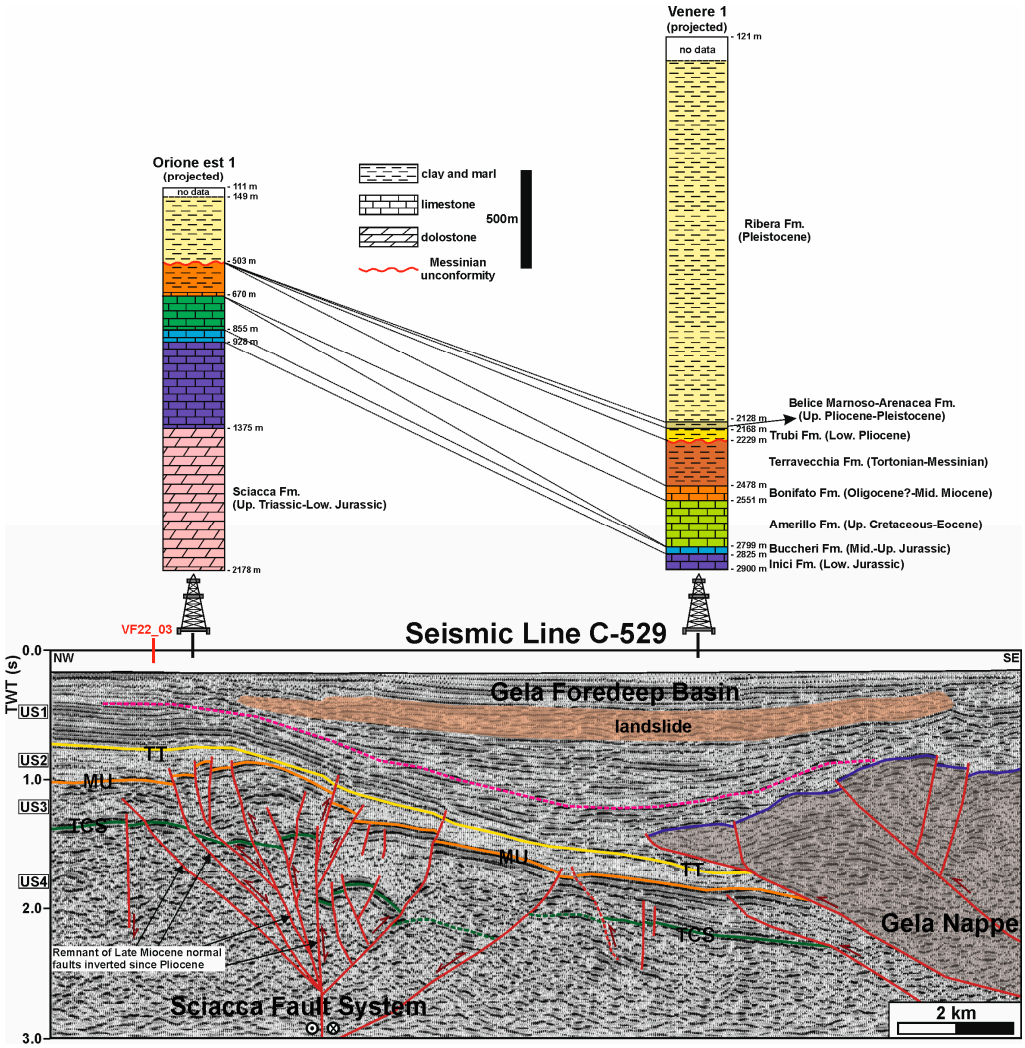

Figure 3. Interpretation of the NW−SE-oriented multichannel seismic reflection profile C−529, located a few kilometers off the Sicilian coast between Capo San Marco and Sciacca (position in Figure 2) and crossing the high-resolution seismic profile VF22_03 in its northern part. This seismic line shows the tectonic setting of the Sciacca offshore, characterized from NW to SE by the NNE−striking left−lateral transpressive Sciacca Fault System, the Gela Foredeep Basin, and the Gela Nappe. The exploration wells Orione Est 1 and Venere 1 (see position in Figure 2) were used to calibrate the interpretation. The first 100 ms of seismic data are lacking along the seismic profile. Abbreviations: MU: Messinian unconformity; TCS: Top of the carbonate succession; TT: Top of the Trubi Fm.; US1: seismo-stratigraphic Unit S1 associated with the upper Pliocene–Pleistocene succession including Ribera and Belice Marnoso-Arenacea formations; US2: seismo-stratigraphic Unit S2 associated with the lower Pliocene Trubi Fm.; US3: seismo-stratigraphic Unit S3 mainly associated with the Tortonian–lower Messinian Terravecchia Fm.; US4: seismo-stratigraphic Unit S4 associated with Mesozoic–Cenozoic carbonate succession. The magenta dashed line within the Unit S1 (US1) succession is an unconformity produced by tectonic activity along the Sciacca Fault System.

4.1.2. Tectonics

Seismic line C-529 images the northernmost part of the NNE-striking, left-lateral transpressional SFS fault system that forms the eastern boundary of the CGSFZ lithospheric shear zone (Figure 3). The SFS consists of a prominent buried positive flower structure, up to about 7 km wide, that affects the Mesozoic–Cenozoic carbonate succession and the siliciclastic Miocene deposits and deforms the Messinian unconformity (Figure 3). Thickness variations in Miocene deposits (Unit S3) between the SFS and surrounding zones indicate that a positive tectonic inversion affected the main faults of the transpressive structure

(Figure 3). Since the Pliocene, transpressional deformation along the SFS has inverted previous late Miocene normal faults [6,8]. Normal displacements are still locally visible. The SFS is still active along its entire length [6,8]. Within succession US1 (upper Pliocene–Quaternary), a major unconformity (black dashed line in Figure 3) can be identified. It is characterized at the top by reflections with onlapping terminations indicating a tectonic uplift episode and an associated bending of the NW margin of the foredeep basin caused by tectonic activity along the Sciacca Fault System. A positive flower structure occurs at Nerita Bank and deforms the seafloor [6], while high-resolution seismic profiles collected in the northernmost part of the SFS show that folding and local minor faulting affect the youngest deposits [6,8]. The transpressional zone generated by the SFS forms the western boundary of the GFB, whose fill hosts a broad, acoustically chaotic body (up to about 200 m thick) in the upper part, interpreted as a landslide deposit (Figure 3). This body was probably generated by the Pleistocene emplacement of the GN [33,49]. The Gela basin exhibits a weakly deformed foredeep depocenter formed during the Plio-Quaternary in response to the flexure of the Pelagian foreland caused by the loading of the GN [47], which is well shown on seismic line C-529 (Figure 3). The SE part of this line shows the buried frontal termination of the Oligocene–Pleistocene GN (Figure 3), which is the outermost and youngest thrust sheet of the Sicilian–Maghrebian chain. The basal thrust of the GN dips toward SE and shows a visible shortening of about 5 km. The GN imaged by the seismic line C-529 consists of two tectonic slices with an antiformal internal architecture separated by a secondary NW-verging thrust (Figure 3).

4.2. High-Resolution Seismic Lines

The six high-resolution seismic profiles acquired in the Capo San Marco–Sciacca offshore area (Figure 2) run on the continental shelf at a water depth between 20 m and 50 m. In the central part of the seismic profile VF22_01, a prominent bank rises to a 12 m water depth. The seismic profiles image the sedimentary succession beneath the seafloor up to about 60 m (65–70 ms TWT), assuming an average interval velocity of 1700 m/s. The interpretation of the three more significant profiles (VF22_00, 01, and 03) has been reported in this paper.

4.2.1. Seismic Stratigraphy

Seismo-stratigraphic analysis allowed the identification of three seismic units, labeled from younger to older as A, B, and C, separated by two well-recognizable erosional unconformities named S1 and S2 (Figures 4–7).

Unit A consists of high-frequency, low- to high-amplitude, parallel reflectors that are laterally continuous (Figure 4). The reflectors are sub-horizontal or slightly inclined and apparently unaffected by tectonic deformation. The maximum thickness of Unit A is about 22 m (27–28 ms TWT), assuming an interval velocity of 1600 m/s [58]. The basal erosional surface S1 is an irregular high-amplitude reflector characterized by minor reliefs and depressions and onlapped or draped by the reflectors of Unit A (Figures 5–7). Surface S1 is interpreted as the LGM (Last Glacial Maximum) unconformity, as already proposed by several authors in this area of the Sicilian Channel [6,8,12,13,51,59–61]. It is a composite surface formed first by subaerial erosion caused by the global glacio-eustatic sea level fall that culminated ca. 20 ka B.P., when the sea level was ca. 120–130 m below the present-day shoreline [62,63], and then by wave action during the post-LGM marine transgression that reworked the subaerial unconformity. According to this interpretation, Unit A is associated with the upper Pleistocene–Holocene sedimentary succession formed during the transgressive and highstand stages of the post-LGM sea level rise.

Unit B is a discontinuous body with a complex architecture and variable thickness, considering an interval velocity of 1700 m/s [58], from a few meters to 12 m (2–18 ms TWT) within prominent U-shaped incisions, filled with a heterogeneous succession and interpreted as paleo-valleys incised during older lowstand phases (Figures 4–7). The seismic facies consists of an alternation of discontinuous and subparallel reflectors of medium- to high-amplitude and medium- to high-frequency and of local chaotic facies (Figure 4). This succession contains minor internal unconformities. Unit B has been interpreted as the result of an amalgamation of regressive and transgressive sediments deposited during glacio-eustatic sea level changes that occurred in the middle-late Pleistocene [8]. The base of Unit B is the erosional surface S2, a prominent high-amplitude reflector that truncates the underlying deformed sedimentary succession and is characterized, as noted above, by the presence of paleo-valleys that deeply incise Unit C (Figures 4–7).

Unit C consists of well-stratified, parallel, continuous low- to medium-amplitude, and high-frequency reflectors (Figure 4) affected by folding and local faulting (Figures 5–7), with an interval velocity of 1800 m/s [6]. Based on literature information [8,9], Unit C is associated with the lower Pleistocene silty clay deposits of the Ribera Fm., which corresponds to the onshore Marsala Fm. [21].

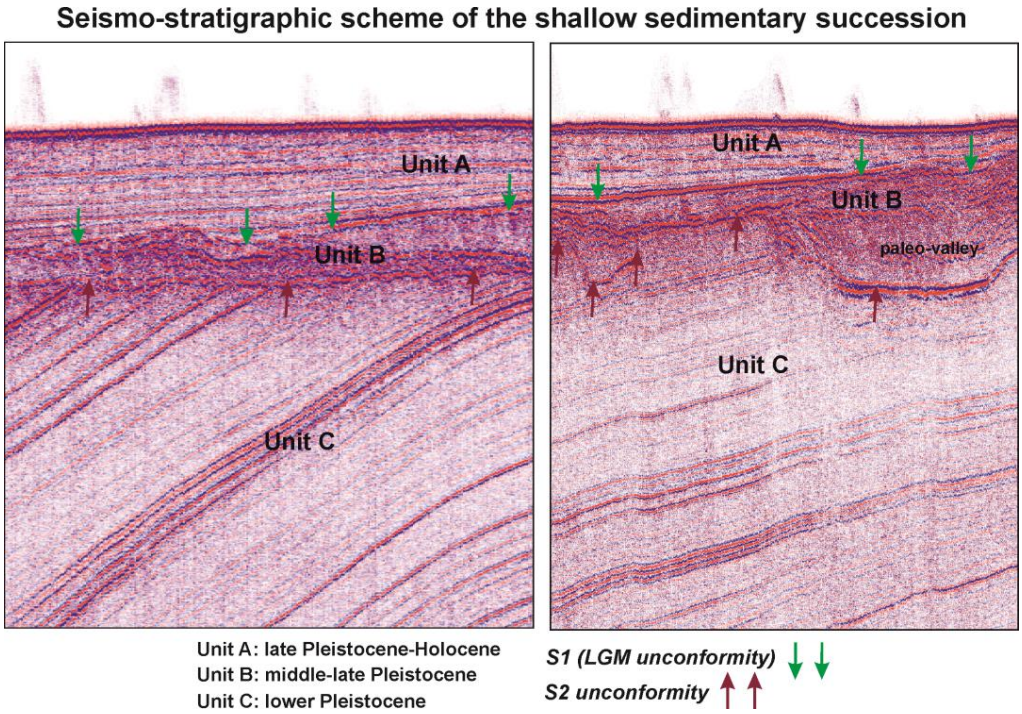

Figure 4. Two representative boxes extracted from the high-resolution seismic lines VF22_00 (**left**) and VF22_03 (**right**) that illustrate the seismo–stratigraphic features of the shallow sedimentary succession of the study area. Three seismic units, labeled A, B, and C, from younger to older, with different facies separated by two well-recognizable erosional unconformities (S1 and S2), have been identified. Their description can be found in the text.

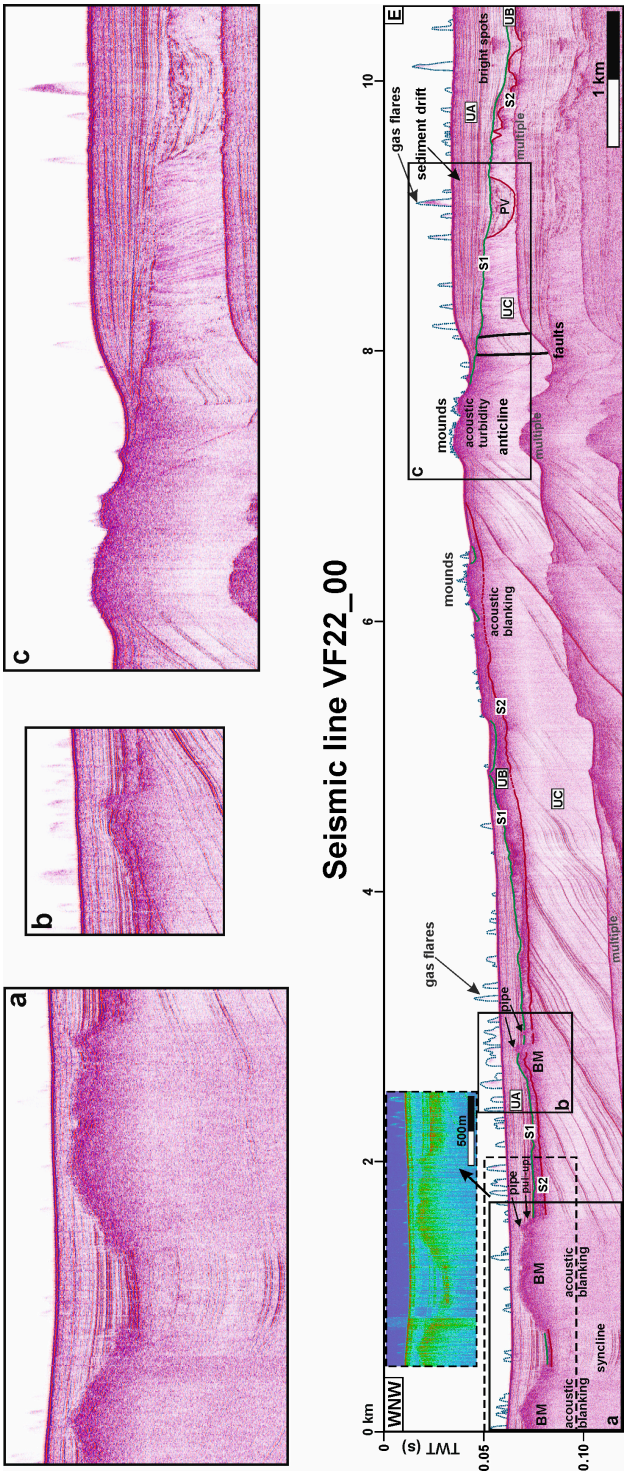

Figure 5. Interpretation of the high-resolution seismic profile (Boomer data) VF22_00 (position in Figure 2b; vertical exaggeration 20×). The colored rectangular inset shows the instantaneous amplitude calculated for the western part of the line (see text for interpretation), which is characterized by the presence of two prominent buried mounds. Above are some details of the seismic line (indicated by the corresponding boxes **a**–**c**). Abbreviations: BM: buried mound; PV: paleo–valley; UA, UB, and UC: seismo–stratigraphic units A, B, and C, respectively, described in the text; S1: high–amplitude reflector associated with the LGM unconformity and located at the base of Unit A; S2: high–amplitude reflector corresponding to an erosional surface at the base of Unit B that truncates the underlying sedimentary succession of Unit C.

4.2.2. Fluid-Related Features

The presence of shallow fluid migration in the high-resolution seismic profiles is supported by several typical fluid-related features associated with seismic signal anomalies (e.g., [12,64–66]), which, for the subsurface, include (Figures 5–7): (i) acoustic turbidity caused by the presence of fluid in the sediment pore space, resulting in poor amplitude and low continuity of reflectors (e.g., [67–69]); (ii) acoustic blanking zones, where the seismic signal is lost, caused by the absorption of acoustic energy by fluid-charged sediment (e.g., [67,68,70]). The difference between acoustic blanking and turbidity is thought to be related to the amount of free fluid accumulated in the sediment [71]; (iii) pipes associated with the upward migration of fluids, which are vertical disturbances hundreds of meters wide, similar to the chimneys, characterized by a poor amplitude chaotic facies caused by the disruption of seismic reflectors due to fluid flow (e.g., [72–78]); and (iv) seismic amplitude anomalies at the top of fluid seepages known as "bright spots". The latter indicate the top of a fluid-charged sediment and are characterized by high-amplitude reverse polarity (e.g., [79]). The bright spot results from the increase in acoustic impedance contrast with the surrounding sediment in which no fluid is present.

Fluid seeps from the seafloor are numerous along all seismic lines (Figures 5–7), but no samples are available. These seeps produce detectable amplitude anomalies in the water column known as flares (e.g., [67–80]), which can be detected.

In addition, several buried and outcropping mounds of varying shapes and sizes associated with fluid expulsion have been identified. These mounds generally exhibit opaque seismic facies that does not allow good signal penetration and sometimes show chaotic facies at the top (Figures 5–7). They are not associated with magnetic anomalies.

4.2.3. Line VF22_00

This seismic line (Figure 5) is about 10.5 km long and shows a roughly E-W orientation (Figure 2b). Its western part is located 2 km from Capo San Marco. The well-layered Unit C (Marsala Fm.) is affected by folding; in particular, the hinge zone of a syncline is partially visible in the westernmost part of the line, while in the eastern part of the line, a kilometer-scale symmetrical anticline forming a structural high is visible (Figure 5). The anticline has a vertical axial surface and an eastern limb affected by several high-angle faults that separate the fold from a zone characterized by steep reflectors. Unit C is deeply eroded in the eastern part of the seismic line by channels and a 500 m wide paleo-valley (Figure 5). Unit B has a variable thickness, reaching a maximum of about 11 m in the paleo-valley fill sediments. A sediment drift at least 2.5 km long and about 22 m thick characterizes Unit A in the eastern part of the seismic line (Figure 5).

Fluid seeps in the water column associated with hydroacoustic flares up to 15 m high are visible along the entire seismic line. Their presence indicates a widespread presence of fluids in the near-surface sedimentary succession. Two groups of mounds can be identified on the seafloor. The eastern group consists of three mounds of different shapes and sizes located on the hinge zone of the anticline (Figure 5). The two eastern mounds of this group show an almost flat top, and their base is not visible. The presence of these mounds causes a zone of acoustic turbidity in Unit C. The largest mound is about 300 m wide and 5 m high and, like the others, has opaque seismic facies. The distinction into two mounds could also be the result of erosion of a previous single mound. The westernmost and smallest mound of the group, characterized by a cone shape, lies on the LGM unconformity or S1 surface and could be related to fluid migration along the underlying fault. All of these mounds are associated with fluid seeps in the water column.

The western group of mounds (located just after kilometer 6) consists of several cone-shaped active mounds a few meters high, covered by fluid seeps and having the same seismic facies as those in the previous group (Figure 5). These mounds lie on both Unit B and Unit A and produce a zone of acoustic blanking.

In the westernmost part of the line (between 0 and 2 km), there are two buried prominent mounds, the larger of which is about 12 m high and up to more than 800 m wide (Figure 5). They are characterized by a very irregular top that is probably the result of repeated phases of subaerial erosion. The complex top morphology does not allow to identify the possible presence of a thin sedimentary cover associated with Unit B. The base of the mounds is not visible, although they probably lie on Unit C. The top of these mounds is covered by about 4–5 m of sediments of Unit A. The presence of these seismically opaque mounds does not allow signal penetration, resulting in zones of acoustic blanking. The reflectors of units A and B terminate in onlap against the flanks of the mounds. A possible active pipe (located at kilometer 1.5) can be seen in the easternmost part of the top of the larger buried mound. This vertical feature produces a pull-up effect on the surrounding reflectors and an overlying deformation zone that terminates near the seafloor. The instantaneous amplitude calculated for these buried mounds shows that their reflectivity at the top is lower than that of the Unit B reflectors (Figure 5). This could be related to the presence of softer sediments.

At kilometer 3, another small, buried mound, which shows the same seismic characteristics as the others, lies on Unit C and is draped by Unit B (Figure 5). An active pipe that deforms the surrounding reflectors is located along its eastern flank.

In the easternmost part of the seismic line, bright spots are visible in the deep part of the sediment drift, indicating the top of fluid-charged sediments (Figure 5).

4.2.4. Line VF22_01

This E-W-oriented seismic line (Figure 6) is about 6.5 km long, and its central part is located 1.3 km from Capo San Marco and is about 500 m north of line VF22_00 (Figure 2b).

The well-layered Unit C is visible only in the western part of the line, where it consists of W-dipping reflectors (Figure 6). In the eastern part of the seismic line, Unit C is deeply eroded by a broad paleo-valley less than 1 km wide and is affected by a zone of acoustic blanking due to the presence of buried mounds (Figure 6). A prominent mound, about 18 m high and 600 m wide, is visible in the central part of the line (Figure 6). It is characterized by an almost flat top and a subvertical eastern flank. The presence of this large mound produces an acoustic blanking zone in Unit C. Several fluid seeps up to 13 m high are visible along the irregular top of the mound, which is the result of repeated periods of subaerial erosion, and particularly along its inclined western flank. Considering the position of this mound, it is likely that it lies on a structural high formed by the same anticline recognized in the line VF22_00. Unlike the previous line, it is not possible to identify different mounds on the top of the structural high. The instantaneous amplitude calculated for this mound shows that the reflectivity of its top is lower than that of the seafloor (Figure 6). This could be related to the presence of an irregular top consisting of softer sediments compared to the surrounding seafloor.

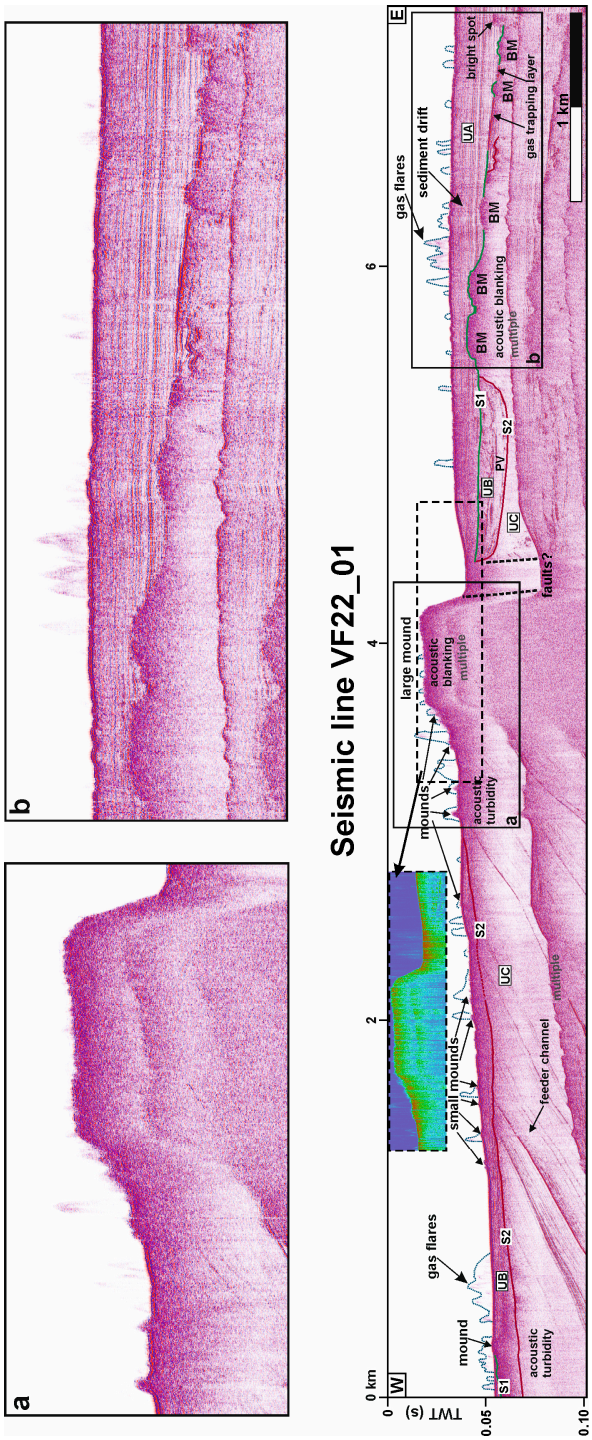

Figure 6. Interpretation of the high–resolution seismic profile (Boomer data) VF22_01 (position in Figure 2b; vertical exaggeration 20×). The colored rectangular inset shows the instantaneous amplitude calculated for the central part of the line (see text for interpretation), which includes the large mound visible at the seafloor and surrounding zones. Above are some details of the seismic line (indicated by the corresponding boxes **a**,**b**). Abbreviations: BM: buried mound; PV: paleo–valley; UA, UB, and UC: seismo-stratigraphic units A, B, and C, respectively, described in the text; S1: high-amplitude reflector associated with the LGM unconformity and located at the base of Unit A; S2: high–amplitude reflector corresponding to an erosional surface at the base of Unit B that truncates the underlying sedimentary succession of Unit C.

Unit B outcrops in the western part of the line with a maximum thickness of about 9–10 m (Figure 6). In the eastern part of the line, Unit B fills the deeply incised paleo-valley, where a maximum thickness of about 12 m is reached, as well as some minor channels (Figure 6). The observed paleo-valley can be correlated with the one visible in line VF22_00. A sediment drift consisting of Unit A is visible in the eastern part of the seismic line for more than 3 km. In this part of the line, the S1 surface associated with the LGM unconformity shows an irregular shape.

Numerous fluid seepages from the seafloor are visible along the seismic line, indicating a widespread occurrence of fluid in the shallow marine sediments. Active small cone-shaped mounds, several meters high and located on Units B and C, are visible on the seafloor in the western part of the line and along the western flank of the large mound (between 0 and about 3.5 km) (Figure 6). They are usually associated with seafloor fluid seeps and locally produce zones of acoustic turbidity in the underlying succession. For one of these mounds, it is possible to detect the vertical feeder channel characterized, by chaotic seismic facies (Figure 6).

A group of buried mounds lying on Unit C is visible below the sediment drift located in the eastern part of the line at different depths between 8 and 16 m below the seafloor (Figure 6). The two larger buried mounds show an almost flat top, probably produced by subaerial erosion, whereas the top of the others exhibits a crater-like shape. The largest buried mound is about 6 m high and 350 m wide. These mounds are characterized by opaque seismic facies, and the reflectors of Unit A terminate in onlap against their flanks. The succession overlying the central mound of these groups shows a gentle antiformal deformation linked to the presence of seafloor fluid seeps. This allows us to hypothesize that it is active.

As in the previous line, a bright spot is visible in the easternmost and deeper part of the sediment drift (Figure 6). Moreover, in this part of the line, the S1 surface is locally characterized by high-amplitude reverse polarity zones, this suggests that the S1 surface may act as a trapping layer for upward fluid migrations from Unit C.

4.2.5. Line VF22_03

This line (Figure 7) is less than 14 km long and connects the Capo San Marco offshore with the Sciacca offshore (Figure 2b). In particular, the northwestern part of the line is about 1 km from the town of Sciacca.

Unit C or Marsala Fm. is affected by a broad asymmetric anticline that extends for at least 7 km (Figure 7). This fold has a steeper eastern limb (forelimb), a less inclined western limb (backlimb), and an east-dipping axial surface. Growth strata, characterized by progressive thinning toward the hinge zone of the anticline, are clearly visible and allow dating of the fold formation to the early Pleistocene. Minor folds are also visible within the western limb of the anticline. The imaged anticline represents the southern extent of the fold visible in line VF22_00 and presumably in line VF22_01, which would have an NNE trending. Unit C is not visible in the eastern part of the seismic line, mainly due to the diffuse presence of fluid causing acoustic blanking (Figure 7). The shape of the top of the Unit C or S2 surface indicates strong erosion, as evidenced by the presence of paleo-valleys and channels filled by Unit B, which have also eroded the crest of the anticline (Figure 7).

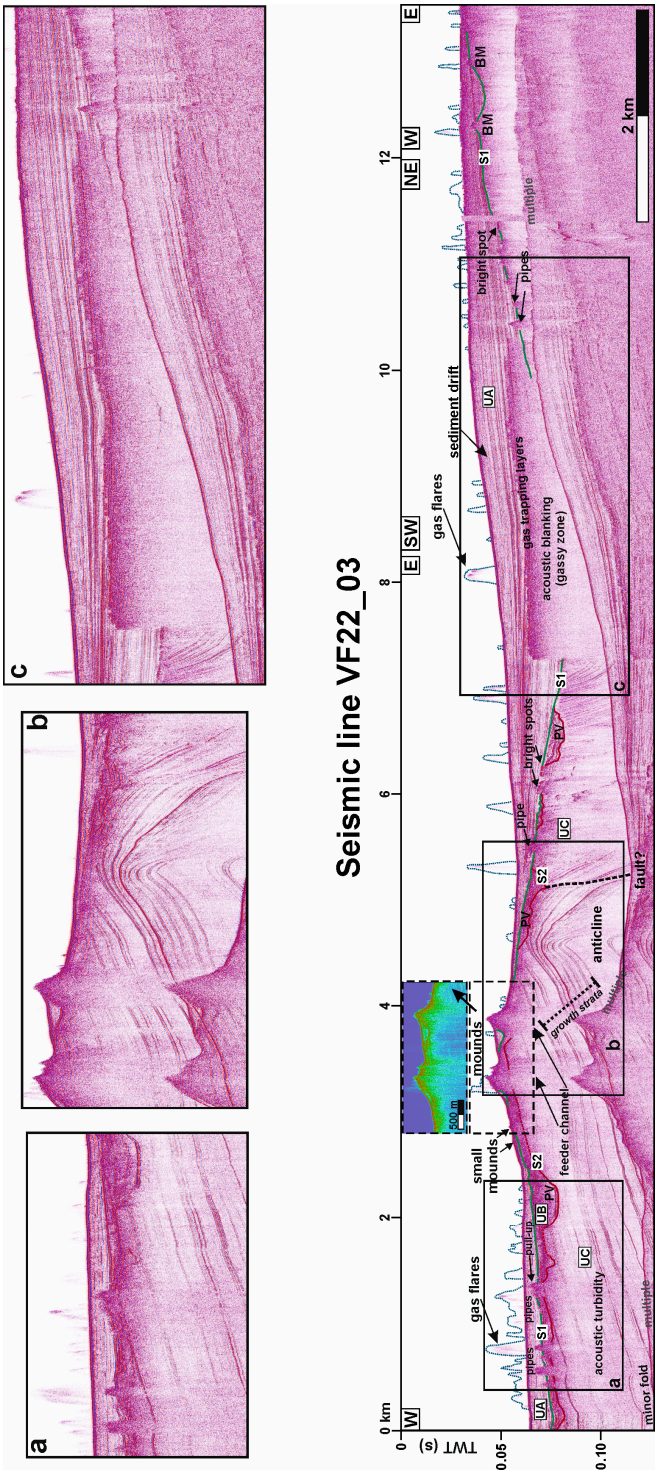

Figure 7. Interpretation of the high–resolution seismic profile (Boomer data) VF22_03 (position in Figure 2b; vertical exaggeration 20×). The colored rectangular inset shows the instantaneous amplitude calculated for the part of the line that includes the two prominent seafloor mounds and surrounding zones (see text for interpretation). Above are some details of the seismic line (indicated by the corresponding boxes **a**–**c**). Abbreviations: BM: buried mound; PV: paleo–valley; UA, UB, and UC: seismo-stratigraphic units A, B, and C, respectively, described in the text; S1: high–amplitude reflector associated with the LGM unconformity and located at the base of Unit A; S2: high–amplitude reflector corresponding to an erosional surface at the base of Unit B that truncates the underlying sedimentary succession of Unit C.

In the western part of the seismic line, Unit B shows significant thickness variations with a maximum of more than 11 m in the westernmost paleo-valley (Figure 7). Unit A is almost absent at the morphological high located between kilometers 3 and 4, whereas in the eastern part, consists ofthe thick sediment drift already documented in the other lines (Figure 7).

Fluid seeps in the water column, up to 18–19 m high, are visible along the entire seismic line. The morphological high visible on the seafloor lies on the western limb of the anticline (Figure 7). It consists of a group of cone-shaped active mounds with two main structures up to 8 m high and about 100 m wide. They exhibit opaque seismic facies and probably lie on Unit B. The surface of the westernmost mound is completely covered by fluid seeps. The presence of these mounds causes a zone of acoustic turbidity in the underlying succession where two feeder channels have been inferred. The instantaneous amplitude calculated for the top of this group of mounds emphasizes its lower reflectivity than that of the seafloor (Figure 7), which is probably related, as well as in the previous seismic lines, to the presence of softer sediments.

The tops of several pipes are identifiable in Unit A west of the morphological high between 0 and 1.5 km (Figure 7). They cause a general degradation of the seismic signal and interrupt the continuity of the seismic reflections affected by pull-up effects near the pipes. In addition, given the presence of an almost continuous fluid seepage zone in the water column, it is likely that these pipes can reach the seafloor. These pipes are fed by fluids that migrated through Unit C.

A fluid-bearing zone about 3 km wide, characterized by a distinct acoustic blanking, is clearly visible beneath the eastern part of the sediment drift (Figure 7). The top of the fluid front is at a variable depth between 10 and 17 m, where there are some fluid-trapping stratigraphic layers of Unit A, which probably consist of fine-grained sediments with low permeability that form a barrier to upward fluid migration. In some places (e.g., between 9 and 9.5 km), the fluid appears to migrate upward beyond the top of the fluid-bearing zone (Figure 7) probably due to variations in sediment properties. In any case, the presence of seepages from the seafloor indicates that some amount of fluid also reaches the surface. Pipes associated with localized deformation of the surrounding sediments, and bright spots, are visible along the base of Unit A, both west and east of the gas-bearing zone (Figure 7). They indicate upward migration of fluid from Unit C. Finally, two small cone-shaped buried mounds, less than 3 m high, are visible in the easternmost part of the seismic line.

5. Discussion

The analysis of the high-resolution seismic lines collected on the Capo San Marco-Sciacca continental shelf of the SGF has shown the widespread presence of shallow active fluid manifestations, such as outcropping and buried mounds, pipes, zones of acoustic blanking and turbidity, bright spots, and a considerable number of seepages of fluids from the seafloor associated with hydroacoustic flares in the water column (Figures 5–7). Thus, upward fluid migration occurs both through focused seepages, likely structurally controlled by faults and fracture zones, and through diffuse flows associated with shallow, unconsolidated, and unfaulted porous marine sediments. In particular, several mounds are located along the hinge zone of a broad lower Pleistocene anticline that is generally affected by pervasive fracturing, while seeps may produce fractures in soft sediment that are not visible on seismic data.

The evidence described suggest that a significant amount of fluid is present in the shallow marine Quaternary sedimentary succession of the Capo San Marco–Sciacca offshore area compared to adjacent areas, which are characterized by more localized phenomena [12,81].

Within the various fluid-related features visible in the study area, the identified mounds remain of doubtful interpretation, also due to the lack of available core data. These positive features, not associated with magnetic anomalies, can be divided into two types (Figures 5–7): (i) active small cone-shaped mounds, generally a few meters high, located on the seafloor and associated with seeps in the water column and (ii) buried and outcropping larger mounds generally characterized by an almost flat top, which, in some

cases, show a very irregular shape. The largest of these mounds is more than 800 m wide and about 12 m high (Figure 5). The seafloor mounds are usually associated with fluid seeps in the water column and the presence of smaller active cone-shaped mounds at the surface, whereas pipes are locally associated with buried mounds. In some cases, feeder channels have been identified for some positive structures of the two groups (Figures 6 and 7).

The largest mounds generally lie on the lower Pleistocene Unit C, associated with the onshore Marsala Fm., and sometimes on the middle-upper Pleistocene Unit B. Based on their features, they are interpreted as submarine structures eroded during the numerous lowstand phases that occurred since the middle Pleistocene. Their size suggests that in the past, larger volumes of fluid were released over long periods of time than today. In addition, the older mounds generally show evidence of current activity, with the exception of the two larger buried structures visible on the seismic line VF22_01 (Figure 6). However, these mounds are located below several fluid seeps from the seafloor, which may indicate that upward fluid migration is still active.

The mound-shaped features are tentatively interpreted as representing mud volcanoes, although a different origin, such as authigenic carbonate mounds (e.g., [82,83]), cannot be completely ruled out. This hypothesis is based on the following literature and seismic data: (i) mud volcanoes and mud diapirs were identified about 7 km north of Capo San Marco [12] and in the Licata offshore, about 40 km eastward from the study area [81]. Shallow marine mud volcanoes have also been reported along the continental shelf of the Malta plateau [84]; (ii) onshore, about 20 km east of the town of Sciacca, mud volcanoes, locally known as "macalube", are reported (e.g., [9]); (iii) wells drilled up to 3000 m in the area of the town of Sciacca show no hydrocarbons and only a small amount of methane [2,9]; and (iv) the observed mounds generally show an opaque seismic facies with no internal reflectors and a top characterized by a low reflectivity (Figures 5–7). In addition, feeder channels were identified in some cases.

In contrast, the carbonate mounds generally exhibit continuous high-amplitude capping reflection and a pull-up effect of the internal reflectors, which can also present contorted to chaotic seismic facies due to the higher seismic velocity of the carbonate strata compared to the siliciclastic strata (e.g., [85–87]).

Evidence obtained from the analysis of the high-resolution seismic profiles suggests that an extensive fluid field was active in the Capo San Marco–San Marco offshore area since the lower Pleistocene, which can be considered the offshore extension of the SGF (Figure 8a). The period of large fluid emission likely coincided with the period of maximum tectonic activity of the area, highlighted by the presence of the broad anticline visible in the three high-resolution seismic profiles presented in this work (Figures 5–7). The NNE-trending anticline, which deforms lower Pleistocene deposits, can be considered the northernmost part of a 17 km long fold known as the Sciacca Anticline North associated with the transpressional faults of the SFS [8]. In this context, the S1 surface, which represents the top of Unit C, could be the result of the sum of the lower Pleistocene tectonics and the onset of the high-magnitude middle Pleistocene glacio-eustatic sea level fall.

Active onshore tectonic deformations affecting late-middle to late Pleistocene marine terraces have also been documented in the Sciacca area [21].

According to the onshore literature [1,2,9,11], the fluid field located in the Capo San Marco–Sciacca offshore area is likely fed by a deep thermal and saline aquifer hosted in Triassic carbonate deposits, as reported for the SGF, and, together, they form a single geothermal field with an extension of about 70 km^2 (Figure 8a). Figure 8a shows the features (both on the seafloor and buried) derived from the analysis and interpretation of the collected seismic data. However, the lack of multibeam coverage of the study area shown in the figure and the sparse distribution of the high-resolution seismic profiles do not allow a complete representation of features that characterize the Sciacca offshore area.

The origin of thermalism and the considerable contribution of mantle gasses in the onshore thermal springs and wells remain to be clarified. The interpretation of the multichannel seismic profile C-529 has shown the presence of a prominent positive flower

structure beneath the offshore fluid field (Figure 3). This structure represents the northern part of the active NNE-striking, left-lateral transpressive SFS, which, together with the CGFS, forms the lithospheric shear zone CGSFZ. According to Calò and Parisi [34], the CGSFZ could extend onshore up to the Tyrrhenian coast of Sicily.

The formation of a geothermal resource and evidence for the presence of mantle gasses from geochemical and isotopic analyses of springs and wells in the SGF presumably presupposes the presence of a heat source, which could be represented by mantle magma that has migrated upwards along the lithospheric tectonic structures of the SFS, heating and contaminating the fluids of the carbonate reservoir (Figure 8b). The SFS faults, which probably also interacted at a shallower level on land with the thrusts of the SFTB, would have acted as preferential pathways for fluid accumulation in the shallow subsurface and seafloor. In support of this, several authors suggested that the origin of the magmatism observed at the Graham and Terrible banks and in the Capo Granitola–Sciacca offshore area was due to the direct ascent of magma along the CGSFZ [6,51]. In this context, the numerous fluids seeping from the seafloor, which are well visible in the high-resolution seismic profiles, could consist of thermal/hot water and/or gasses.

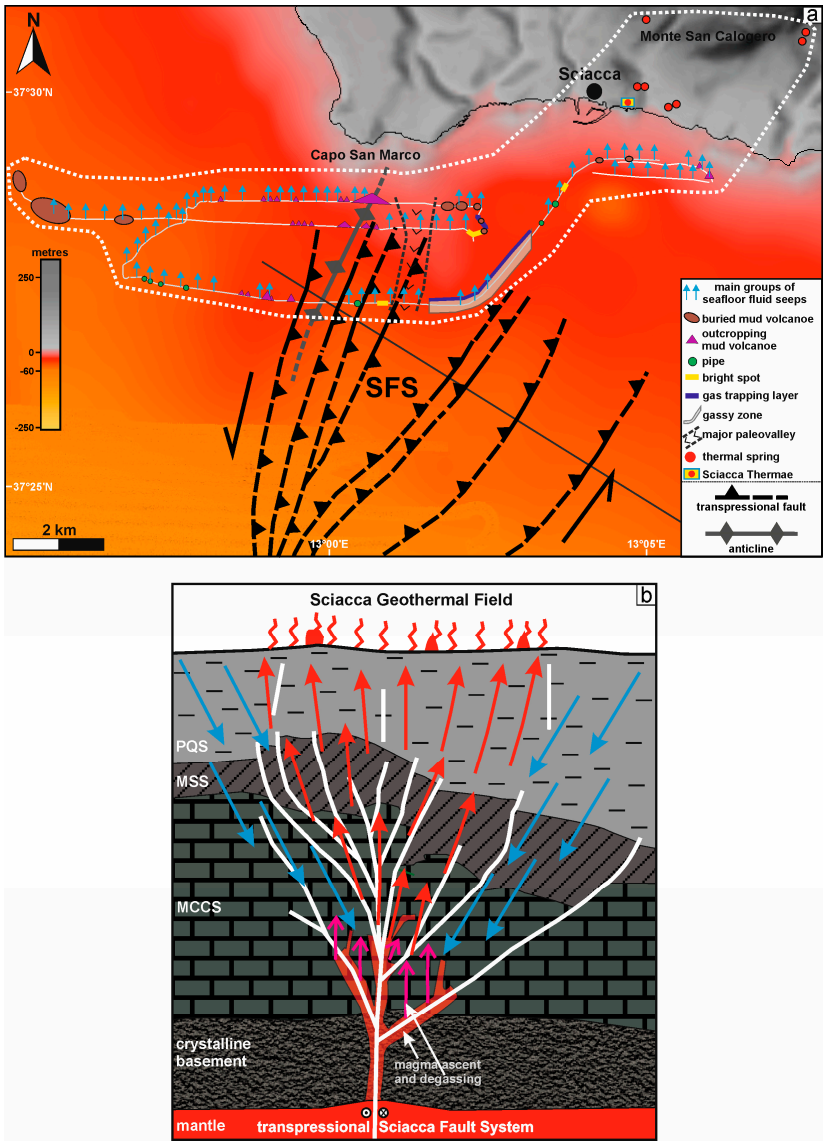

Figure 8. (**a**) Map showing the location of the main fluid-related features identified along the high–resolution seismic profiles (thin white lines) in the Capo San Marco–Sciacca offshore area and the position of the positive flower structure associated with the NNE–striking left-lateral transpressive

Sciacca Fault System (SFS) interpreted along MCS line C–529 (thin grey line) (see Figure 3 for interpretation). The location of the main thermal springs and Sciacca Thermae is also indicated. The white dotted curve represents the documented onshore–offshore extent of the Sciacca Geothermal Field based on the data presented in this paper. Morpho-bathymetric data from the EMODnet Bathymetry Portal (http://emodnet-bathymetry.eu/) Digital Terrain Model (1/16*1/16 arcmin grid resolution) and multibeam data acquired by OGS. (**b**) Schematic model showing the plausible mechanism for the formation of the Sciacca Geothermal Field. This field has developed in a tectonically active zone dominated by the left–lateral transpressive structures associated with the lithospheric, NNE–striking SFS. The presence of these faults may have favored the rising of magma (in red) and fluids (magenta arrows) from the mantle in the Capo San Marco–Sciacca offshore area and the consequent heating of groundwater (blue arrows), leading to the formation of a geothermal resource contained in the Triassic carbonate succession outcropping on the Monte San Calogero. Theis cold water (red arrows) rises to the surface. Abbreviations: MCCS: Mesozoic–Cenozoic Carbonate Succession; MSS: Miocene Siliciclastic Succession; PQS: Pliocene–Quaternary Succession.

6. Conclusions

Geophysical analysis of newly acquired high-resolution seismic profiles (Boomer data), integrated by a multichannel seismic reflection profile, has made it possible to document the presence of generally active shallow fluid-related features (pipes, bright spots, buried and outcropping mud volcanoes, zones of acoustic blanking, and seafloor fluid seeps) in the Capo San Marco–Sciacca offshore area and to reveal the deep tectonic structure of this sector. The studied area is located in close proximity to the onshore SGF, which is characterized by hot water containing mantle gasses.

The hot springs of the SGF and the diffuse submarine fluid-related features likely form a single onshore–offshore fluid field of thermal origin, encompassing an area of at least 70 km^2. This field has developed in a tectonically active zone dominated by a left-lateral transpressive regime associated with the lithospheric, NNE-striking SFS. The faults associated with the SFS probably favored the rising of magma and fluids from the mantle in the Capo San Marco–Sciacca offshore area, leading to the formation of a geothermal resource hosted in the Triassic carbonate succession (Figure 8b), which crops out on land in the Monte San Calogero. This field has been active since the lower Pleistocene, during which time fluid emissions were likely greater than today and were associated with greater SFS tectonic activity that led to the formation of the broad anticline visible in the high-resolution seismic profiles. The results of this work should stimulate further studies aimed at investigating the composition and temperature of the seafloor fluid seeps, determining the actual extent of the offshore part of the geothermal field, and the possible presence of biological communities associated with the seeps and mounds. In this way, the potential for low-enthalpy energy production in the Sciacca area can be reassessed, and the potentially identified benthic communities could lead to the creation of a new marine protected area.

Author Contributions: Conceptualization, marine data analysis and interpretation, D.C. and M.Z.; original draft preparation, D.C.; investigation, L.B., D.C. and E.L.; formal analysis, L.B.; data curation, D.C., L.B. and F.A.; review and editing, D.C., M.Z. and F.A.; visualization, D.C., F.A., N.M., V.V., G.M.F. and M.B. All authors have read and agreed to the published version of the manuscript.

Funding: This research received no external funding.

Institutional Review Board Statement: Not applicable.

Informed Consent Statement: Not applicable.

Data Availability Statement: The C-529 multichannel seismic reflection profile and well data used for the presented research are made available in the ViDEPI project (Visibility of Petroleum Exploration Data in Italy) of the Italian Ministry of the Economic Development: "http://www.videpi.com". The presented morpho-bathymetric data are from the EMODnet Bathymetry Portal:

"http://emodnet-bathymetry.eu/". The three high-resolution seismic profiles (Boomer data) reported in the manuscript and acquired by OGS in October 2022 are available in SEGY format on request from the corresponding author.

Acknowledgments: The authors thank the crew of the patrol boat CC-811 "Pignatelli" (Trapani) of the Italian "Arma dei Carabinieri" for their help in collecting data at sea. Suggestions and comments from two anonymous reviewers have helped to improve the manuscript considerably.

Conflicts of Interest: The authors declare no conflict of interest.

References

1. Aureli, A. Bacino Termale di Sciacca (Sicilia S.O.). In *Caratteristiche Idrogeologiche e Vulnerabilità*; CNR, Quaderni di Tecniche di Protezione Ambientale; Pitagora Editrice: Bologna, Italy, 1996; Volume 59, p. 168.
2. Capaccioni, B.; Vaselli, O.; Tassi, F.; Santo, A.P.; Delgado Huertas, A. Hydrogeochemistry of the thermal waters from the Sciacca Geothermal Field (Sicily, southern Italy). *J. Hydrol.* **2011**, *396*, 292–301. [CrossRef]
3. Ogniben, L. Schema introduttivo alla geologia del confine calabro-lucano. *Mem. Soc. Geol. It.* **1969**, *8*, 453–763.
4. Argnani, A.; Cornini, S.; Torelli, L.; Zitellini, N. Neogene-Quaternary foredeep system in the Strait of Sicily. *Mem. Soc. Geol. It.* **1986**, *36*, 123–130.
5. Argnani, A. The Strait of Sicily rift zone: Foreland deformation related to the evolution of a back-arc basin. *J. Geodyn.* **1990**, *12*, 311–331. [CrossRef]
6. Civile, D.; Lodolo, E.; Accaino, F.; Geletti, R.; Schiattarella, M.; Giustiniani, M.; Fedorik, J.; Zecchin, M.; Zampa, L. Capo Granitola-Sciacca Fault Zone (Sicilian Channel, Central Mediterranean): Structure vs magmatism. *Mar. Pet. Geol.* **2018**, *96*, 627–644. [CrossRef]
7. Civile, D.; Brancolini, G.; Lodolo, E.; Forlin, E.; Accaino, F.; Zecchin, M.; Brancatelli, G. Morphostructural setting and tectonic evolution of the central part of the Sicilian Channel (central Mediterranean). *Lithosphere* **2021**, *2021*, 7866771. [CrossRef]
8. Ferranti, L.; Pepe, F.; Barreca, G.; Meccariello, M.; Monaco, C. Multi-temporal tectonic evolution of Capo Granitola and Sciacca foreland transcurrent faults (Sicily Channel). *Tectonophysics* **2019**, *765*, 187–204. [CrossRef]
9. Montanari, D.; Minissale, A.; Doveri, M.; Gola, G.; Trumpy, E.; Santilano, A.; Manzella, A. Geothermal resources within carbonate reservoirs in western Sicily (italy): A review. *Earth-Sci. Rev.* **2017**, *169*, 180–201. [CrossRef]
10. Caracausi, A.; Favara, R.; Italiano, F.; Nuccio, P.M.; Paonita, A.; Rizzo, A. Active geodynamics of the central Mediterranean sea: Heat and helium evidences for a transtensional zone connecting the Sicily Channel to the southern Tyrrhenian Sea. *Geophys. Res. Lett.* **2005**, *32*, L04312. [CrossRef]
11. Donato, A.; Tassi, F.; Pecoraino, G.; Manzella, A.; Vaselli, O.; Candela Gagliano, E.; Santilano, A.; La Pica, L.; Scaletta, C.; Capecchiacci, F. Geochemical investigations of the geothermal systems from the Island of Sicily (southern Italy). *Geothermics* **2021**, *95*, 102120. [CrossRef]
12. Ferrante, G.M.; Accaino, F.; Civile, D.; Lodolo, E.; Volpi, V.; Romeo, R.; Accettella, D. Deep and shallow gas occurrence in the NW Sicilian Channel and related features. *Mar. Pet. Geol.* **2022**, *139*, 105575. [CrossRef]
13. Volpi, V.; Civile, D.; Lodolo, E.; Romeo, R.; Accettella, D.; Accaino, F.; Ferrante, G.M. Seabed and shallow morphological setting of the western Sicilian Channel. *Bull. Geophys. Oceanogr.* **2022**, *63*, 357–376. [CrossRef]
14. Sibson, R.H. Structural permeability of fluid driven fault-fracture meshes. *J. Struct. Geol.* **1996**, *18*, 1031–1042. [CrossRef]
15. Curewitz, D.; Karson, J.A. Structural settings of hydrothermal outflow: Fracture permeability maintained by fault propagation and interaction. *J. Volcanol. Geotherm. Res.* **1997**, *79*, 149–168. [CrossRef]
16. Dewey, J.F.; Helman, M.L.; Knott, S.D.; Turco, E.; Hutton, D.H.W. Kinematics of the western Mediterranean. *Geol. Soc. Spec. Pub.* **1989**, *45*, 265–283. [CrossRef]
17. Roure, F.; Howell, D.G.; Moretti, I.; Müller, C. Neogene subduction complex of Sicily. *J. Struct. Geol.* **1990**, *12*, 259–266. [CrossRef]
18. Gueguen, E.; Doglioni, C.; Fernandez, M. On the post-25 Ma geodynamic evolution of the western Mediterranean. *Tectonophysics* **1998**, *298*, 259–269. [CrossRef]
19. Faccenna, C.; Becker, T.W.; Pio Lucente, F.; Jolivet, L.; Rossetti, F. History of subduction and back-arc extension in the Central Mediterranean. *Geophys J. Int.* **2001**, *145*, 809–820. [CrossRef]
20. Carminati, E.; Lustrino, M.; Doglioni, C. Geodynamic evolution of the central and western Mediterranean: Tectonics vs. igneous petrology constraints. *Tectonophysics* **2012**, *579*, 173–192. [CrossRef]
21. Ferranti, L.; Burrato, P.; Selchi, D.; Andreucci, S.; Pepe, F.; Pascucci, V. Late Quaternary coastal uplift of southwestern Sicily, central Mediterranean sea. *Quat. Sci. Rev.* **2021**, *255*, 106812. [CrossRef]
22. Barreca, G.; Bruno, V.; Cocorullo, C.; Cultrera, F.; Ferranti, L.; Guglielmino, F.; Guzzetta, L.; Mattia, M.; Monaco, C.; Pepe, F. Geodetic and geological evidence of active tectonics in south-western Sicily (Italy). *J. Geodyn.* **2014**, *82*, 138–149. [CrossRef]
23. Di Stefano, P.; Vitale, F. *Carta Geologica dei Monti Sicani Occidentali, Scala 1:50.000*; Univeristà degli Studi di Palermo, Dipartimento di Geologia e Geodesia, Stampa Pezzino: Palermo, Italy, 1993.
24. Ruggieri, G.; Unti, A.; Unti, M.; Moroni, M.A. La calcarenite di Marsala (Pleistocene Inferiore) e i terreni contermini. *Boll. Soc. Geol.* **1975**, *94*, 1623–1655.

25. Di Maggio, C.; Agate, M.; Contino, A.; Basilone, L.; Catalano, R. Unconformity bounded stratigraphic units of Quaternary deposits mapped for the CARG Project in northern and western Sicily. *Alp. Mediterr. Quat.* **2009**, *22*, 345–364.
26. Alaimo, R.; Tonani, F. *Il Bacino Termale di Sciacca—Nota III, Geotermometria delle Acque Termali e Modello di Miscuglio per le Acque Emergenti*; Risorse Termali Della Sicilia e Isole Minori: Palermo, Italy, 1984; pp. 3–18.
27. Gemmellaro, C. Sopra la fisionomia delle montagne di Sicilia, cenno geologico. *Atti Acc. Gioenia Sci.* **1831**, *5*, 73.
28. Gemmellaro, C. Relazione dei fenomeni del nuovo vulcano sorto dal mare fra la costa di Sicilia e l'isola di Pantelleria nel mese di luglio 1831. *Atti Acc. Gioenia Sci.* **1833**, *8*, 271–298.
29. Hoffmann, F. Observations faites pendant un voyage en Sicile. *Bull. Soc. Geol. De France* **1833**, *3*, 70.
30. Alaimo, R.; Carapezza, M.; Dongarrà, G.; Hauser, S. Geochimica delle sorgenti termali siciliane. *Rend. Soc. Mineral. Petrol.* **1978**, *34*, 577–590.
31. Favara, R.; Grassa, F.; Inguaggiato, S.; Valenza, M. Hydrogeochemistry and stable isotopes of thermal springs: Earthquake-related chemical changes along Belice Fault (Western Sicily). *Appl. Geochem.* **2001**, *16*, 1–17. [CrossRef]
32. Antonelli, M.; Franciosi, R.; Pezzi, G.; Querci, A.; Ronco, G.P.; Vezzani, F. Paleogeographic evolution and structural setting of the northern side of the Sicily Channel. *Mem. Soc. Geol.* **1988**, *41*, 141–157.
33. Ghisetti, F.C.; Gorman, A.R.; Grasso, M.; Vezzani, L. Imprint of foreland structure on the deformation of a thrust sheet: The Plio-Pleistocene Gela Nappe (southern Sicily, Italy). *Tectonics* **2009**, *28*, TC4015. [CrossRef]
34. Calò, M.; Parisi, L. Evidences of a lithospheric fault zone in the Sicily Channel continental rift (southern Italy) from instrumental seismicity data. *Geophys. J. Int.* **2014**, *199*, 219–225. [CrossRef]
35. Fedorik, J.; Toscani, G.; Lodolo, E.; Civile, D.; Bonini, L.; Seno, S. Structural analysis and Miocene-to-present tectonic evolution of a lithospheric-scale, transcurrent lineament: The Sciacca Fault (Sicilian Channel, Central Mediterranean Sea). *Tectonophysics* **2018**, *722*, 342–355. [CrossRef]
36. Palano, M.; Ursino, A.; Spampinato, S.; Sparacino, F.; Polonia, A.; Gasperini, L. Crustal deformation, active tectonics and seismic potential in the Sicily Channel (Central Mediterranean), along the Nubia-Eurasia plate boundary. *Sci. Rep.* **2020**, *10*, 21238. [CrossRef]
37. Argnani, A.; Cornini, S.; Torelli, L.; Zitellini, N. Diachronous foredeep-system in the neogene-quaternary of the Strait of Sicily. *Mem. Soc. Geol. It.* **1987**, *38*, 407–417.
38. Argnani, A. Neogene tectonics of the Strait of Sicily. In *Geological Development of the Sicilian-Tunisian Platform*; Max, M.D., Colantoni, P., Eds.; UNESCO Report in Marine Science; University of Urbino: Urbino, Italy, 1993; Volume 58, pp. 55–60.
39. Argnani, A. Neogene basins in the Strait of Sicily (Central Mediterranean): Tectonic settings and geodynamic implications. In *Recent Evolution and Seismicity of the Mediterranean Region*; Boschi, E., Mantovani, E., Morelli, A., Eds.; Kluwer Academic Publication: Dordrecht, The Netherlands, 1993; pp. 173–187. [CrossRef]
40. Grasso, M. The Apenninic-Maghrebian orogen in southern Italy, Sicily and adjacent areas. In *Anatomy of an Orogen: The Apennines and Adjacent Mediterranean Basins*; Vai, G.B., Martini, I.P., Eds.; Kluwer Academic Publishers: Norwell, MA, USA, 2001; pp. 255–286. [CrossRef]
41. Lentini, F.; Carbone, S.; Guarnieri, P. Collisional and postcollisional tectonics of the Apenninic-Maghrebian Orogen (Southern Italy). In *Post-Collisional Tectonics and Magmatism in the Eastern Mediterranean Region*; Dilek, Y., Pavlides, S., Eds.; Geological Society of America Special Paper; The Geological Society of America: Boulder, CO, USA, 2006; Volume 409, pp. 57–81. [CrossRef]
42. Catalano, R.; Franchino, A.; Merlini, S.; Sulli, A. A crustal section from the Eastern Algerian basin to the Ionian ocean (Central Mediterranean). *Mem. Soc. Geol. It.* **2000**, *55*, 71–85.
43. Civile, D.; Lodolo, E.; Alp, H.; Ben-Avraham, Z.; Cova, A.; Baradello, L.; Accettella, D.; Burca, M.; Centonze, J. Seismic stratigraphy and structural setting of the Adventure Plateau (Sicily Channel). *Mar. Geophys. Res.* **2014**, *35*, 37–53. [CrossRef]
44. Catalano, R.; Infuso, S.; Sulli, A. The Pelagian Foreland and its northward Foredeep. Plio-Pleistocene structural evolution. In *Geological Development of the Sicilian-Tunisian Platform*; Max, M.D., Colantoni, P., Eds.; UNESCO Report in Marine Science; University of Urbino: Urbino, Italy, 1993; Volume 58, pp. 37–42.
45. Lickorish, W.H.; Grasso, M.; Butler, R.W.H.; Argnani, A.; Maniscalco, R. Structural styles and regional tectonic setting of the "Gela Nappe" and frontal part of the Maghrebian thrust belt in Sicily. *Tectonics* **1999**, *18*, 655–668. [CrossRef]
46. Butler, R.W.H.; Grasso, M.; La Manna, F. Origin and deformation of the neogene recent maghrebian foredeep at the Gela Nappe, SE Sicily. *J. Geol. Soc.* **1992**, *149*, 547–556. [CrossRef]
47. Catalano, R.; Di Stefano, P.; Sulli, A.; Vitale, F.P. Paleogeography and structure of the Central Mediterranean: Sicily and its offshore area. *Tectonophysics* **1996**, *260*, 291–323. [CrossRef]
48. Catalano, R.; Valenti, V.; Albanese, C.; Accaino, F.; Sulli, A.; Tinivella, U.; Gasparo Morticelli, M.; Zanolla, C.; Giustiniani, M. Sicily's fold–thrust belt and slab roll-back: The SI.RI.PRO. seismic crustal transect. *J. Geol. Soc.* **2013**, *170*, 451–464. [CrossRef]
49. Cavallaro, D.; Monaco, C.; Polonia, A.; Sulli, A.; Di Stefano, A. Evidence of positive tectonic inversion in the north-central sector of the Sicily Channel (Central Mediterranean). *Nat. Hazards* **2017**, *86*, S233–S251. [CrossRef]
50. Coltelli, M.; Cavallaro, D.; D'Anna, G.; D'Alessandro, A.; Grassa, F.; Mangano, G.; Patanè, D.; Gresta, S. Exploring the submarine Graham Bank in the Sicily Channel. *Ann. Geophys.* **2016**, *59*, S0208. [CrossRef]
51. Lodolo, E.; Civile, D.; Zecchin, M.; Zampa, L.S.; Accaino, F. A series of volcanic edifices discovered a few kilometers off the coast of SW Sicily. *Mar. Geol.* **2019**, *416*, 105999. [CrossRef]

52. Lodolo, E.; Renzulli, A.; Cerrano, C.; Calcinai, B.; Civile, D.; Quarta, G.; Calcagnile, L. Unreveling past submarine eruptions by dating lapilli tuff-encrusting coralligenous (Actea Volcano, NW Sicilian Channel). *Front. Earth Sci.* **2021**, *9*, 664591. [CrossRef]
53. Cavallaro, D.; Coltelli, M. The Graham volcanic field offshore southwestern Sicily (Italy) revealed by high-resolution seafloor mapping and ROV images. *Front. Earth Sci.* **2019**, *7*, 311. [CrossRef]
54. Washington, H.S. The submarine eruption of 1831 and 1891 near Pantelleria. *Am. J. Sci.* **1909**, *27*, 131–150. [CrossRef]
55. Colantoni, P.; Del Monte, M.; Gallignani, P.; Zarudzki, E.F.K. Il Banco Graham: Un vulcano recente del Canale di Sicilia. *Giorn. Geol.* **1975**, *40*, 141–162.
56. Di Stefano, E.; Infuso, S.; Scarantino, S. Plio-Pleistocene sequence stratigraphy of south western offshore Sicily from well-logs and seismic sections in a high resolution calcareous plankton biostratigraphic framework. In *Geological Development of the Sicilian-Tunisian Platform*; Max, M.D., Colantoni, P., Eds.; UNESCO Report in Marine Science; University of Urbino: Urbino, Italy, 1993; Volume 58, pp. 105–110.
57. Cohen, J.K.; Stockwell, J.W. *CWP/SU: Seismic Un*x Release No. 42: An Open Source Software Package for Seismic Research and Processing*; Center for Wave Phenomena, Colorado School of Mines: Golden, CO, USA, 2010.
58. Meccariello, M. Tectonic evolution and current deformation of the NW Sicily Channel and the Lampedusa Plateau based on multi-resolution seismic profiles analysis. Ph.D. Thesis, Univeristy of Naples Federico II, Naples, Italy, 2017; p. 261. Available online: http://www.fedoa.unina.it/12119/ (accessed on 5 March 2018).
59. Civile, D.; Lodolo, E.; Zecchin, M.; Ben-Avraham, Z.; Baradello, L.; Accettella, D.; Cova, A.; Caffau, M. The lost Adventure Archipelago (Sicilian Channel, Mediterranean Sea): Morpho-bathymetry and Late Quaternary palaeogeographic evolution. *Glob. Planet. Change* **2015**, *125*, 36–47. [CrossRef]
60. Civile, D.; Lodolo, E.; Caffau, M.; Baradello, L.; Ben-Avraham, Z. Anatomy of a submerged archipelago in the Sicilian Channel (central Mediterranean Sea). *Geol. Mag.* **2016**, *153*, 160–178. [CrossRef]
61. Lodolo, E.; Galassi, G.; Spada, G.; Zecchin, M.; Civile, D.; Bressoux, M. Post-LGM coastline evolution of the NW Sicilian Channel: Comparing high-resolution geophysical data with Glacial Isostatic Adjustment modeling. *PLoS ONE* **2020**, *15*, e0228087. [CrossRef]
62. Siddall, M.; Rohling, E.J.; Almogi-Labin, A.; Hemleben, C.; Meischner, D.; Schmelzer, I.; Smeed, D.A. Sea-level fluctuations during the last glacial cycle. *Nature* **2003**, *423*, 853–858. [CrossRef]
63. Clarke, P.U.; Dyke, A.S.; Shakum, J.D.; Carlson, A.E.; Clark, J.; Wohlfarth, B.; Mitrovica, J.X.; Hostetler, S.W.; McCabe, A.M. The last glacial maximum. *Science* **2009**, *325*, 710–714. [CrossRef] [PubMed]
64. Kim, Y.-J.; Cheong, S.; Chun, J.-H.; Cukur, D.; Kim, A.-P.; Kim, J.-K.; Kim, B.-Y. Identification of shallow gas by seismic data and AVO processing: Example from the southwestern continental shelf of the Ulleung Basin, East Sea, Korea. *Mar. Pet. Geol.* **2020**, *117*, 104346. [CrossRef]
65. Horozal, S.; Chae, S.; Kim, D.H.; Seo, J.M.; Lee, S.M.; Han, H.S.; Cukur, D.; King, G.-S. Seismic evidence of shallo gas in sediments on the southeastern continental shelf of Korea, east Sea (Japan Sea). *Mar. Pet. Geol.* **2021**, *133*, 105291. [CrossRef]
66. Ma, G.; Zhan, L.; Lu, H.; Hou, G. Structures in shallow marine sediments associated with gas and fluid migration. *J. Mar. Sci. Eng.* **2021**, *9*, 396. [CrossRef]
67. Judd, A.G.; Hovland, M. The evidence of shallow gas in marine sediments. *Cont. Shelf Res.* **1992**, *12*, 1081–1095. [CrossRef]
68. Schroot, B.M.; Klaver, G.T.; Schüttenhelm, R.T.E. Surface and subsurface expressions of gas seepage to the seabed—Examples from the Southern North Sea. *Mar. Pet. Geol.* **2005**, *22*, 499–515. [CrossRef]
69. Gay, A.; Lopez, M.; Berndt, C.; Séranne, M. Geological controls on focused fluid flow associated with seafloor seeps in the Lower Congo Basin. *Mar. Geol.* **2007**, *244*, 68–92. [CrossRef]
70. Lee, M.W.; Dillon, W.P. Amplitude blanking related to the pore-fillingof gas hydrate in sediments. *Mar. Geophys. Res.* **2001**, *22*, 101–109. [CrossRef]
71. Baltzer, A.; Tessier, B.; Nouzé, H.; Bates, R.; Moore, C.; Menier, D. Seistec seismic profile: A toll to differentiate gas signatures. *Mar. Geophys. Res.* **2005**, *26*, 235–245. [CrossRef]
72. Davis, A.M. Shallow gas: An overview. *Continent. Shelf Res.* **1992**, *12*, 1077–1079. [CrossRef]
73. Schroot, B.M.; Schüttenhelm, R.T.E. Shallow gas and gas seepage: Expressions on seismic and other acoustic data from the Netherlands North Sea. *J. Geochem. Explor.* **2003**, *78*, 305–309. [CrossRef]
74. Judd, A.G.; Hovland, M. *Seabed Fluid Flow: The Impact of Geology, Biology and the Marine Environment*; Cambridge University Press: Cambridge, UK, 2007; p. 475. [CrossRef]
75. Moss, J.L.; Cartwright, J. 3D seismic expression of km-scale fluid escape pipes from offshore Namibia. *Basin Res.* **2010**, *22*, 481–501. [CrossRef]
76. Huuse, M.; Jackson, C.A.L.; Van Rensbergen, P.; Davies, R.J.; Flemings, P.B.; Dixon, R.J. Subsurface sediment remobilization and fluid flow in sedimentary basins: An overview. *Basin Res.* **2010**, *22*, 342–360. [CrossRef]
77. Løseth, H.; Gading, M.; Wensaas, L. Hydrocarbon leakage interpreted on seismic data. *Mar. Pet. Geol.* **2009**, *26*, 1304–1319. [CrossRef]
78. Løseth, H.; Wensaas, L.; Arntsen, B.; Hanken, N.-M.; Basire, C.; Graue, K. 1000 m long gas blow-out pipes. *Mar. Pet. Geol.* **2011**, *28*, 1047–1060. [CrossRef]
79. Sheriff, R.; Geldart, L. *Exploration Seismology*, 2nd ed.; Cambridge University Press: Cambridge, UK, 1995; p. 416.

80. Naudts, L.; Batist, M.D.; Greinert, J.; Artemov, Y. Geo- and hydro-acoustic manifestations of shallow gas and gas seeps in the Dnepr paleodelta, northwestern Black Sea. *Lead. Edge* **2009**, *28*, 1030–1040. [CrossRef]
81. Mancuso, M.R.; Catalano, R. Evidenze sismostratigrafiche di fenomeni da espulsione di fluidi, superficiali e profondi, nell'offshore tra Sciacca e Agrigento (*Sicilia meridionale*). *Mem. Descr. Carta Geol. d'It.* **2020**, *105*, 97–102.
82. Aloisi, G.; Bouloubassi, I.; Heijs, S.K.; Pancost, R.D.; Pierre, C.; Sinninghe Damsté, J.S.; Gottschal, J.C.; Forney, L.J.; Rouchy, J.-M. CH_4-consuming microorganisms and the formation of carbonate crusts at cold seeps. *Earth Planet. Sci. Lett.* **2002**, *203*, 195–203. [CrossRef]
83. Mazzini, A.; Ivanov, M.K.; Parnell, J.; Stadnitskaia, A.; Cronin, B.T.; Poludetkina, E.; Mazurenko, L.; van Weering, T.C.E. Methane-related authigenic carbonates from the Black Sea: Geochemical characterisation and relation to seeping fluids. *Mar. Geol.* **2004**, *212*, 153–181. [CrossRef]
84. Holland, C.W.; Etiope, G.; Milkov, A.V.; Michelozzi, E.; Favali, P. Mud volcanoes discovered offshore Sicily. *Mar. Geol.* **2003**, *199*, 1–6. [CrossRef]
85. Burgess, P.M.; Winefield, P.; Minzoni, M.; Elders, C. Methods for identification of isolated carbonate buildups of isolated carbonate reflection data. *AAPG Bull.* **2013**, *97*, 1071–1098. [CrossRef]
86. Donda, F.; Civile, D.; Forlin, E.; Volpi, V.; Zecchin, M.; Gordini, E.; Merson, B.; De Santis, L. The northernmost Adriatic Sea: A potential location for CO_2 geological storage? *Mar. Pet. Geol.* **2013**, *42*, 148–159. [CrossRef]
87. Slonka, L.; Krzywiec, P. Seismic characteristics and development of the Upper Jurassic carbonate buildups from the Miechów Trough (Southern Poland). *Geosciences* **2020**, *10*, 239. [CrossRef]